OPTICAL FIBER FABRY-PEROT SENSOR BASED ON A SINGLEMODE-HOLLOW CORE-SINGLEMODE FIBER STRUCTURE FOR DIRECT DETECTION OF PHASE TRANSITION IN N-OCTADECANE

Wei Han[1], Marek Rebow[2], Dejun Liu[3], Gerald Farrell[1], Qiang Wu[4] and Yuliya Semenova[1]

[1]Photonics Research Centre, Technological University Dublin, Kevin Street, Dublin 8, Ireland

[2]College of Engineering and Built environment, Technological University Dublin, Ireland

[3]Key Laboratory of Optoelectronic Devices and Systems of Ministry of Education and Guangdong Province, College of Physics and Optoelectronic Engineering, Shenzhen University, Shenzhen 518060, China

[4]Department of Mathematics, Physics and Electrical Engineering, Northumbria University, Newcastle Upon Tyne, NE1 8ST, United Kingdom

Key words: Optical fiber sensor, Phase change materials (PCMs), n-octadecane

Abstract

An optical fiber Fabry-Perot sensor to monitor the solid-liquid and liquid-solid phase changes in n-octadecane is investigated. The sensor probe is fabricated by splicing a short section of a hollow core fiber between two single-mode fibers. Light from a broadband source launched into the probe experiences multiple reflections as it travels towards the cleaved end of the probe immersed in the material sample and then back to the detector, creating an output interference spectrum with multiple interference dips. The phase change of the material sample in the vicinity of the fiber probe results in changes of various parameters acting upon the probe (such as temperature, strain or bending) which in turn cause changes in the output interference spectrum. By analyzing the changes in the output spectrum of the probe, such as spectral shift of a selected interference dip, the phase change within a material sample in the vicinity of the fiber probe can be accurately detected. This work is useful for providing a better understanding of the phase change mechanism in phase-change materials (PCMs) and for in-situ phase change detection in PCM-based energy storage systems.

Introduction

Solid-liquid phase change materials (PCMs) demonstrate a strong capability of absorbing or releasing large amounts of energy during phase changes [1] and as a result they are widely used in energy storage applications. However, the phase change temperature varies under different conditions, including air pressure and PCM composition. Thus, detecting the phase changes in-situ is very important for the accurate modelling of materials' behavior, and for better understanding of the phase change mechanism in such materials. Moreover, in practice it is often desirable to monitor the phase change process in order to ensure the most efficient energy storage, therefore, detecting the phase change in-situ is also very important for applications of

PCMs in the energy storage area. Conventional analytical techniques including temperature measurement [2], direct observation [3], X-ray radiography [4] and differential scanning calorimetry (DSC) [5] can be used to detect the phase changes within the material in laboratory conditions. However, each of these methods suffers from specific disadvantages. For example, direct observation of the phase change can only be applied to optically transparent materials. X-ray radiography can be used in both transparent and opaque materials, but it is a laboratory-based method involving high cost equipment. DSC is a very popular technique to detect phase changes, but it does not allow for phase change monitoring at a specific point within the sample's volume, and thus is unsuitable for the energy storage applications which involve large PCM volumes. Temperature measurement is the most popular indirect measurement approach, but it is not always reliable due the phenomenon referred to as supercooling, when the material remains in a liquid state at a temperature below its solidification point.

In the last couple of decades, the optical fiber sensing technology has been a research hotspot as it provides high sensitivity and reliability for the measurements. Optical fiber sensors offer many advantages over their electronic counterparts including high accuracy and sensitivity, small size and light weight, immunity to electromagnetic interference, ability to operate remotely and to provide access into normally inaccessible areas. Optical fiber sensors are explosion proof and resistant to ionizing radiation, they can operate in harsh environments and can be easily interfaced with data communication systems. Many examples of fiber sensor applications for measurements of temperature, strain, stress, vibrations, as well as chemical and biological quantities have been reported recently. Min *et al.* [6] proposed a fiber Sagnac interferometer for temperature sensing. The Sagnac structure sensor head was fabricated by using a section of photonic crystal fiber (PCF) which was filled with ethanol. Compared to a typical Sagnac fiber sensor based on PCF, filling the PCF with ethanol increased the birefringence and temperature sensitivity. The sensitivity was up to 16.66 nm/°C. Mao *et al.* [7] proposed a fiber Fabry Perot (FP) interferometer for temperature measurement. The sensor was fabricated by splicing a section of a single-mode fiber (SMF) with a hollow-core fiber (HCF) filled with polydimethylsiloxane, to form an air microbubble cavity. This sensor had a temperature sensitivity of 2.70 nm/°C, which was three times higher than that of a conventional all-fiber air-cavity FP temperature sensor.

In addition to the temperature measurement, fiber sensors are also applied in strain sensing. Zhao *et al.* [8] proposed a strain sensor based on a tapered fiber Bragg grating (FBG). The sensor head was fabricated by inserting a tapered fiber with an FBG in a capillary and splicing the other end of the capillary with an SMF. This sensor has a high strain sensitivity of 1129.4 pm/με. Sun *et al.* [9] proposed a Mach-Zehnder interferometric (MZI) fiber sensor for strain monitoring with a high strain sensitivity of 42.5 pm/με. The sensor was fabricated by splicing a multimode fiber (MMF) with two SMFs and then the MMF section was heated and twisted. Fiber sensors are often applied for sensing of multiple parameters simultaneously. For example, Song *et al.* [10] proposed a fiber sensor for strain and temperature. The sensor was fabricated by splicing a section of MMF with two SMFs to form a single mode-multimode-single mode (SMS) sensor head, and then writing an FBG into the middle MMF section. Since the SMS spectrum and the FBG spectrum had different sensitivities to strain and temperature, by observing the interference dips from the SMS spectrum and the dip associated with the FBG, the temperature and strain could be detected simultaneously. Several previous reports illustrated that optical fiber sensors can be successfully applied to detection of phase changes

in various materials. For example, Chai *et al.* [11] used a combination of coating-stripped and coated fiber FBG sensors to monitor the solid-liquid and liquid-gas phase transitions in water. Their proposed technique requires a minimum of two FBGs and their different positions within the sample sometimes result in errors. Mani *et al.* [12] proposed a Fresnel reflection fiber sensor for the detection of crystallization of $CaCl_2$-H_2O. In our previous study [13], we developed a Fresnel fiber sensor for detecting the phase changes within n-octadecane. The main shortcoming of such a Fresnel sensor is that it requires at least two measurements to correctly interpret the phase state of the n-octadecane sample. To overcome this, we developed a singlemode-no-core-singlemode (SNS) structure fiber sensor [14]. In comparison with the Fresnel sensor, the SNS sensor allows for the detection of the phase state based on a single measurement of the optical power reflected by the probe. However, both the Fresnel and the SNS sensors operate under the condition that the refractive index (RI) of the sample changes discontinuously during the phase transition and thus are not suitable for detection of phase changes in materials whose RI changes in a continuous manner.

In this paper a new Fabry-Perot fiber sensor is proposed and experimentally demonstrated for the detection of solid-liquid and liquid-solid phase changes in n-octadecane. Compared to our previous work [13-14], the application of the proposed sensor is not limited by the RI of the PCMs. As illustrated in Fig.1, the sensor probe is fabricated by splicing a short section of a HCF, with a length in the order of microns, between two SMFs, to form a single-mode-hollow core-single-mode (SHS) Fabry-Perot structure. Light from a broadband optical source launched into the input SMF (SMF-1) experiences multiple reflections due to RI differences at the interfaces between the SMF-1 and HCF, between the HCF and the second SMF section (SMF-2) and between the end face of SMF-2 and the material under test. The portion of light reflected back from the end face of SMF-2, as a result of Fresnel reflection at the fiber-PCM interface, travels through the same series of interfaces in the reverse direction creating an output interference spectrum which contains multiple interference dips. Any phase changes of the material sample in the vicinity of the fiber probe result in changes in the various parameters acting upon the probe (such as temperature, strain or bending) which in turn will cause the shift of the output interference spectrum. With the probe immersed into the material sample the phase change is detected by monitoring the wavelength shift of the selected interference dip.

Due to its specific thermal characteristics, n-octadecane (C18H38 n-alkane material) is widely used in a number of applications, such as thermal control in spacecraft [15], maintaining temperature in smart textiles [16] and in solar thermoelectric generators [17]. In this work n-octadecane was chosen for a proof-of-principle demonstration of the proposed fiber sensor because the material's phase change occurs in a narrow temperature range and with high degree of repeatability. In addition, the closeness of the freezing point to room temperature allows for a significant simplification of the experimental set up. Moreover, the material is transparent in the liquid phase and becomes opaque in solid phase, which makes it possible to visually observe the phase change in the vicinity of the probe for comparison with the sensor reading. Detecting the phase change in n-octadecane is also helpful for validation of numerical models of phase transitions in similar materials [18]. Although the RI of the n-octadecane changes in a step-like manner when the material undergoes the solid-liquid phase transition, the sensor proposed here is based on an FP structure which is fabricated in a manner so that that the sensor is unaffected by local RI changes but is influenced by the changes in stress placed on the sensor by the solid phase. By monitoring the spectrum is possible to distinguish between the solid and

liquid phases and thus to determine the solidification temperature point. It is shown that the method proposed in this work can be used for accurate in-situ detection of liquid-solid and solid-liquid phase changes in n-octadecane, without the need for RI measurements. This point-sensing technique could in principle be expanded by increasing the number of sensor probes to create a sensor array for detecting the phase changes at multiple points within the PCM sample. For example, in studies and optimization of heat distribution within a volume of PCM material employed in an energy storage system.

Experimental setup and operating principle

The experimental setup for the demonstration of the proposed sensor is shown in Fig. 1. Port 1 of the circulator is connected to a broadband light source (BBS, S5FC1005S(P), Thorlabs), while port 2 is connected with the fiber sensor probe and port 3 is connected to an optical spectrum analyzer (OSA Q8384, Advantest). The probe is fabricated from a very short (300 μm) section of a HCF (10 μm inner air core diameter, 126 μm outer silica cladding diameter) with its coating removed. The HCF section is "sandwiched" between two sections of a standard SMF (SMF-1 and SMF-2) by means of fusion splicing. Due to the limitations of the fiber cleaver, 300 μm is the shortest length of the HCF fiber fabricated in our experiments, but even a shorter length could potentially be obtained. The length of SMF-2 is 1 cm. The protective fiber coating is removed from a small area near the end of SMF-1 then spliced with the sensor probe and this area is marked with blue ink. Since the liquid sample is transparent while the solid sample is not, visual observation of the blue mark indicates that at this point the sample is in the liquid phase. The temperature in the vicinity of the fiber probe was monitored with a K- type thermocouple. The thermocouple was fixed close to the probe. A Peltier element placed at the bottom of the container filled with n-octadecane was used as a thermoelectric heater/cooler.

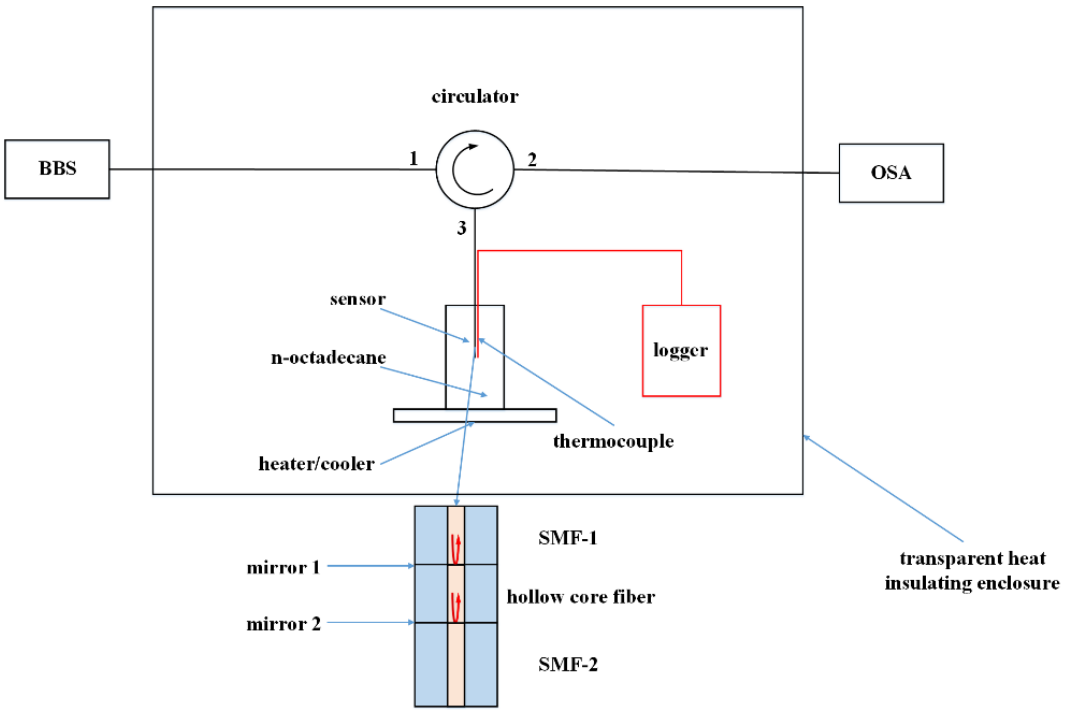

Fig. 1. Schematic diagram of the experimental setup.

Light from the BBS, launched in the SMF-1, experiences partial reflections at the interfaces between SMF-1 and HCF (mirror 1) and HCF and SMF-2 (mirror 2). A portion of light reflected at mirror 2 is re-coupled back in the SMF-1 where it interferes with the light reflected by mirror 1. In the meanwhile, a part of the input light transmitted through mirror 2 experiences further reflections at the end face of SMF-2. Some of the light reflected from the end face of SMF-2 is re-coupled back into the HCF where it interferes with light reflected by mirror 2. It should be noted that SMF-1 is effectively a connecting fiber and its length does not have any effect on the spectrum because it does not form a part of the Fabry-Perot cavity.

As shown schematically in Fig. 1, the HCF section spliced between the two SMFs can be considered as an air cavity with the ends of SMF-1 and SMF-2 acting as cavity mirrors (mirror 1 and 2). The SMF-2 forms the second cavity, where reflections occur at mirror 2 and the cleaved end of the SMF-2 acting as the third mirror. Thus the entire structure can be viewed as two cascaded Fabry-Perot interferometers (FPIs). The free spectral range (FSR) of an FPI is determined as [19]:

$$FSR = \frac{\lambda_1 \lambda_2}{2nL}, \tag{1}$$

where λ_1 and λ_2 are the wavelengths of any two adjacent dips in the interference spectrum, n and L are the RI and the length of the FPI cavity respectively. From equation (1) one can see that the longer is the FP cavity, the smaller is its FSR.

The sensor proposed in this paper is composed of two interferometric cavities, associated with the HCF and SMF-2. For the HCF cavity, the value of n is the RI of the HCF core (air) and L is the length of the HCF. For the SMF-2 cavity, the value of n is the RI of the SMF core and L is the length of the SMF-2. Using equation (1) the corresponding FSRs for both interferometers at a central wavelength of 1550 nm are estimated as ~8 nm for the HCF (given its length of ~300 µm and n = 1) and 0.11 nm for the SMF-2 (assuming the length of 1.5 cm and n = 1.45).

To better understand the properties of the proposed fiber structure the effect of length of SMF-2 on the reflection spectrum was investigated. Three fiber structure samples were fabricated as follows: three samples with the HCF circa 300 µm were selected, whose SMF-2 lengths were 1 cm, 1.5 cm and 2 cm respectively. The length of the SMF-2 establishes the optical path difference between the light reflected by interfaces 2 and 3. Fig. 2 shows the experimentally measured spectra for the above samples with different SMF-2 lengths normalized to the spectrum of the optical source (power ratio (dB)).

From Fig. 2 it can be seen that both estimated values for the FSRs agree well with the experiment and that changes in the length of the SMF-2 section do not significantly affect the fiber probe's spectrum, which means that the effect of the FPI formed by the SMF-2 can be neglected. This is because the SMF-2 is much longer than HCF, so the FSR of the FP cavity associated with SMF-2 is too small to be clearly seen in the spectrum. The dips in the interference spectrum are associated with the FP cavity formed by the HCF. Note that the vertical axes in Fig. 2 and Fig. 3 are in dB rather than dBm as they both show spectra normalized to the input spectrum of the BBS.

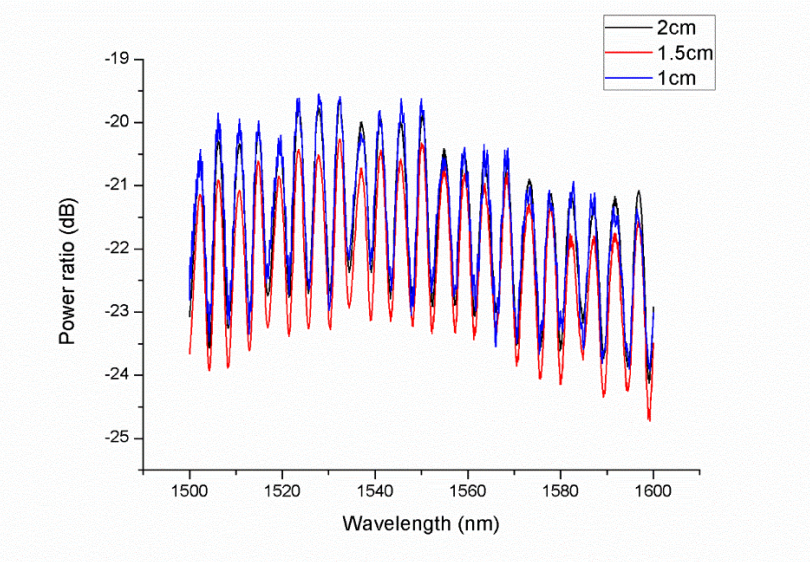

Fig.2 Experimental spectra of the fiber probes with different lengths of SMF-2 normalized to the spectrum of the optical source.

In further experiments the lengths of the HCF and SMF-2 were set to 300 μm and 1 cm respectively, and a typical output spectrum of the structure is shown in Fig. 3.

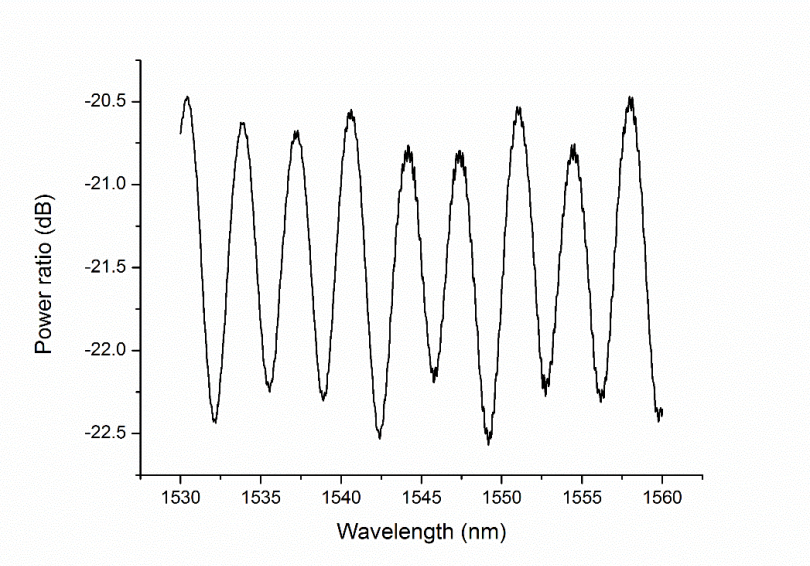

Fig.3 Typical experimental reflected spectrum of the sensor probe, normalized to the spectrum of the optical source.

Due to the variations in the environment surrounding the fiber probe, the length of the HCF cavity may change. Besides, as the environmental temperature changes, the temperature and the pressure of the core of the HCF may also change, changing the effective RI for the modes propagating within the HCF core. The spectral shifts of the interference dips as described as [20] are given by:

$$\Delta\lambda = \lambda\left(\frac{\Delta n}{n} + \frac{\Delta L}{L}\right) \tag{2}$$

where λ is the central wavelength of a selected dip, Δn and ΔL are the variations of the RI and the length of the air cavity respectively. Assuming that only the temperature of the surrounding the probe environment changes, equation (2) can be differentiated as:

$$\frac{d\lambda}{dT} = \lambda\left(\frac{1}{n}\frac{dn}{dT} + \frac{1}{L}\frac{dL}{dT}\right) = \lambda(\delta + \alpha) \quad (3)$$

where δ is the effective thermo-optic coefficient and α is the effective thermal expansion coefficient of the HCF. From equation (3) it can be seen that the wavelength shift of the selected dip caused by temperature variations is a linear function of temperature.

As it can be seen in the Fig.3, the spectrum has a strong periodic component, the lowest point in each period is regarded as an interference dip. When the fiber probe is surrounded by the material in solid phase, changes in the material density associated with the moving liquid phase front result in randomly directed strain and bending forces acting upon the probe causing the non-monotonic spectral shift of the interference dips [21-23]. Since the speed of the liquid phase front propagation may vary at different points within the sample, the direction and amplitude of the strain and the bending forces acting on the sensor probe are random in nature, resulting in a non-monotonic wavelength shift of the interference dips within the reflected spectrum. As soon as the sensor becomes fully immersed in liquid, the strain and the bending forces, significant in the solid phase, become negligibly weak so that the influence of temperature dominates the changes in the spectral positions of the interference dips, leading to a linear behaviour consistent with the temperature response of the probe, determined above.

Therefore analyzing the temperature dependence of the wavelength shift of a selected spectral dip within the sensor's reflection spectrum, it is possible to determine the temperature point at which the nature of the dependence changes from non-monotonic to linear with a certain slope (or vice versa in the case of liquid to solid transition), thus the phase change can be detected.

Experimental results and discussion

As a first step towards the phase change experiments, the temperature dependence of a selected spectral dip was investigated. The spectral dip at 1549 nm was chosen for this purpose as it is the dip with the most pronounced extinction ratio, making it easily observable. The temperature response of the fiber probe was measured using the experimental setup shown in Fig. 2. To provide an initial reference for later experiments, water was used at this point as the material sample instead of n-octadecane. The water sample was heated from 20 ºC to 30 ºC in 1 ºC steps and the corresponding changes in the spectral position of the selected interference dip were recorded. The measurement result is shown in Fig. 4, from which it is observed that the temperature response is approximately linear and the temperature sensitivity of the probe is estimated as 0.006 nm/ºC. It should be noted that since the water sample does not undergo a phase change within the temperature range, the observed spectral shift of the interference spectrum is solely due to the temperature induced change in the HCF's core RI caused by the thermo-optic effect, and the changes in the size of the HCF caused by thermal expansion.

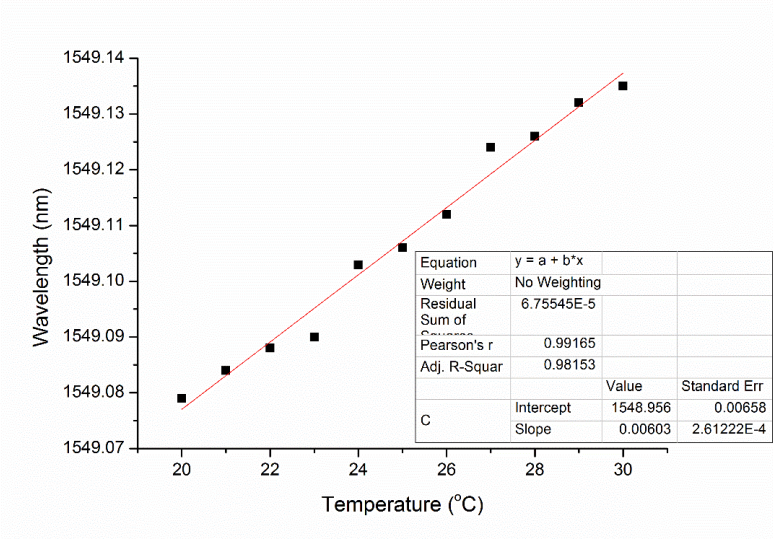

Fig.4 Temperature response of the sensor probe in water.

In order to experimentally demonstrate the operation of the proposed sensor, a series of heating and cooling experiments were carried out for a 25 ml sample of n-octadecane with 99% purity (Sigma Aldrich) in a cuvette with the diameter of 3 cm and height of 4 cm, using the same experimental setup. Both the fiber probe and the thermocouple were immersed into the n-octadecane sample with an approximate 2 mm distance between them. The thermocouple was connected to a logger to record the temperature of the n-octadecane in close proximity of the fiber sensor probe. To ensure stability of the surrounding temperature, the experimental setup was placed inside a transparent heat insulating enclosure. A photo camera was placed inside the enclosure and connected with a laptop for recording images. The camera's shutter was controlled by a PC and a photo image was taken each time the wavelength of the selected dip and temperature data were recorded.

The results of the heating experiment are shown in Fig. 5. The heating experiment was carried out by setting the temperature of the Peltier element to 50 °C causing progressive melting of the sample from the bottom of the cuvette so that the liquid phase front propagated slowly upwards through the sample, where the temperature of surrounding environment was set as 20 °C to ensure a well-defined sharp interface between the solid and liquid n-octadecane. As can be seen from Fig. 5 (a) in the temperature range from 25 °C to 30 °C, the wavelength shift of the selected spectral dip is distinctly non-monotonic by comparison to the temperature response curve in water in the temperature range from 27.5 °C to 28.5 °C. As one can see in Fig. 5, it is linear when the temperature is above 28.5 °C, and the slope of the linear section of the temperature dependence is 0.0058 nm/°C, which is very close to the temperature sensitivity (slope) measured in water. Below 27.5 °C the slope is opposite in sign to the slope above 28.5 °C. This is due to the fact that before the material melts into liquid, as the temperature increases, the combined effects of the multi-directional strain forces acting upon the sensor are the primary cause of the wavelength shift of the selected dip. Since the strain and bending forces come from the variation in the material's density and the speed of the liquid phase front propagation, these forces may vary at different points within the sample, the direction and amplitude of the strain and the bending applied on the fiber causes a distinct wavelength shift which is very different from the linear spectral responses observed below 27.5 °C and above 28 °C. Once the material sample becomes liquid, the strain forces acting upon the fiber become

weaker and more uniform and the surrounding temperature becomes the dominant factor. By recording the spectral response changes with temperature, the change from a solid to a liquid phase can be distinguished and thus from Fig. 5 it can be seen that the phase change of the sample occurs at 28.5 °C. Fig. 6 presents a series of photos that show the gradual movement of the interface between liquid and solid phases during the heating experiment. It can be seen that the sensor is immersed in a solid when the temperature is 28 °C and becomes surrounded by liquid at 28.5 °C, confirming that the 28.5 °C is the phase change point.

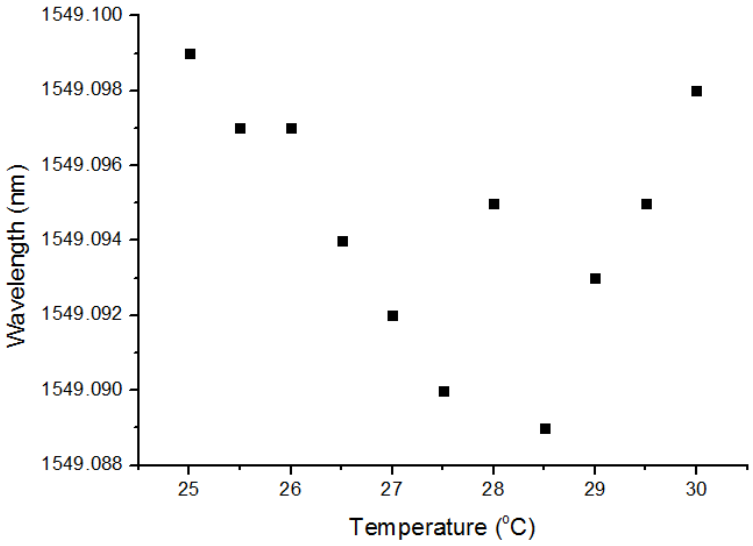

(a)

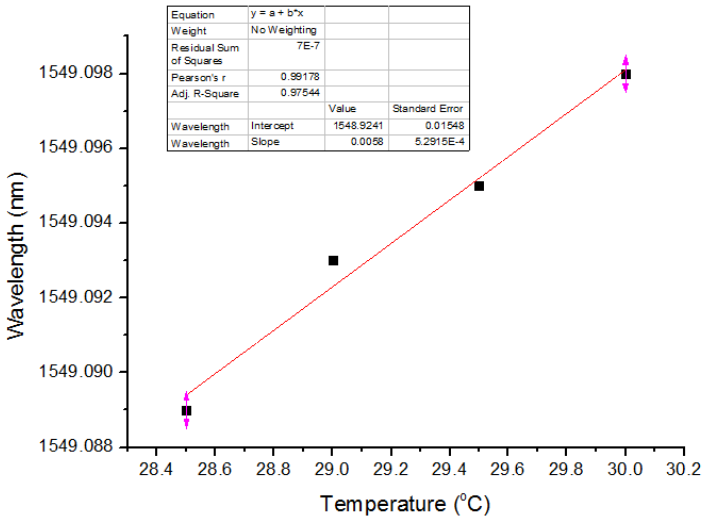

(b)

Fig.5 Results of the heating experiment: (a) selected dip wavelength shift during the heating cycle; (b) dip wavelength shift after the sample melts into liquid.

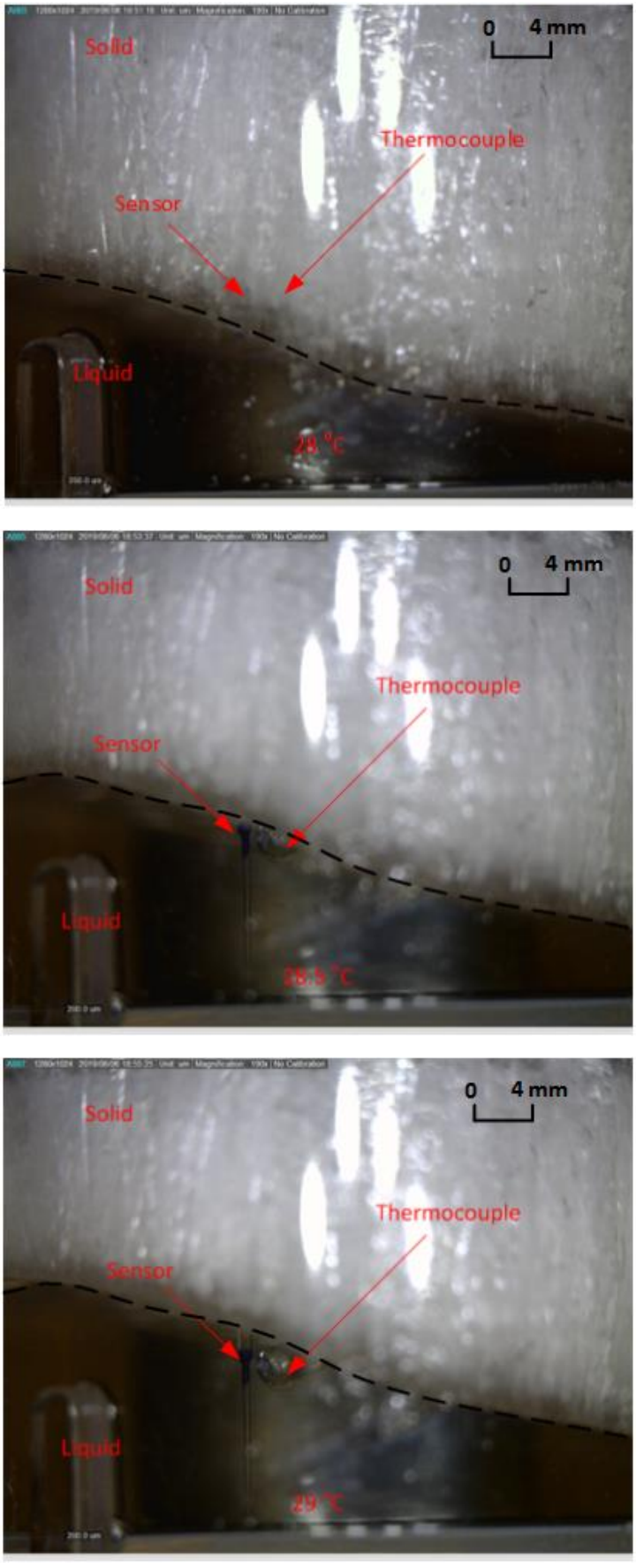

Fig.6 Photographs of the solid-liquid interface position at different temperatures: at 28.5 °C both the thermocouple and fiber optic probe tips are clearly visible.

For the cooling experiment the current direction within the Peltier heater was reversed so that the cold side of the heater was in contact with the sample, causing solidification from the bottom of the cuvette slowly upwards through the sample and again produced a visible interface between the liquid and solid phases that was recorded by the camera. The temperature of the Peltier element was set to 10 °C, while the temperature of the surrounding was set to 30 °C to ensure a well-defined sharp interface between the solid and liquid n-octadecane. The result is shown in Fig.7. From Fig.7 (b) it can be seen that in the temperature range from 30 °C to 28 °C the wavelength shift is linear and the slope is 0.0062 nm/°C, which is very close to the temperature response of the probe in water. This is due to that when the temperature is higher than 28 °C, the sample is in a liquid phase, and the wavelength position of the dip is affected only by temperature. From 27.5 °C to 24 °C the changes in the spectral position of the selected dip become discontinuous, as the Fig.7 (a) shows. When the temperature becomes lower than 28 °C, the sample is surrounded by solidified PCM material. In the solid phase as the temperature decreases, the strain forces acting upon the sensor increase due to the increased density of the material, resulting in randomly directed stress and bending of the fiber probe, resulting in non-linear behaviour of the selected dip. From Fig. 7(a) it can be seen that the phase change occurs at 28 °C on cooling. Fig. 8 shows the gradual movement of the interface between liquid and solid phases during the cooling experiment. The sensor is immersed in liquid when the temperature is 28 °C while it immersed in a solid phase when the temperature is 27.5 °C, which confirms the result of the the fiber probe experiment. The phase change temperature in the cooling experiment is lower than the phase change temperature in the heating experiment due to the known small thermal hysteresis of n-octadecane. For the sensor immersed in the solid phase, the wavelength shifts corresponding to the heating and cooling cycles are different because the strain and bending changes during each cycle are different, so the wavelength shift is not repeatable. However since the rate of the wavelength shift for a sensor immersed in liquid phase is highly repeatable, the phase change point can be accurately detected.

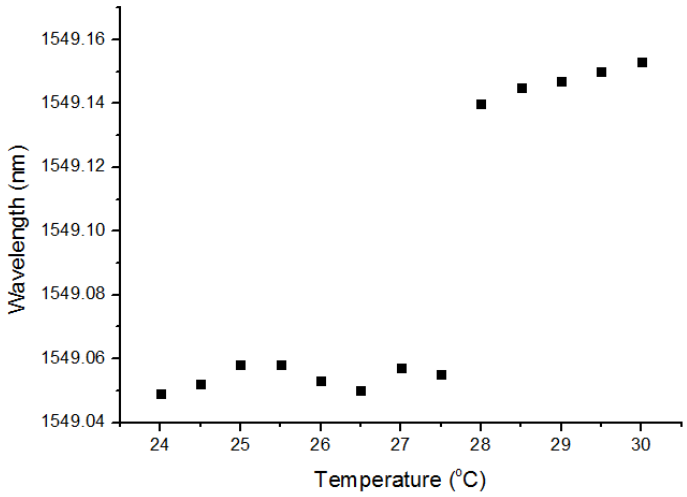

(a)

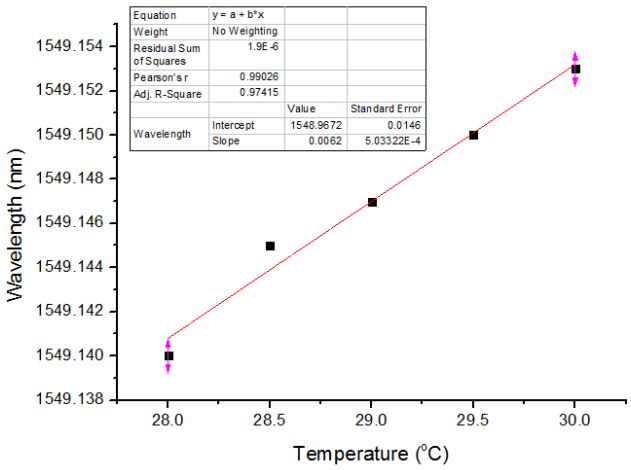

(b)

Fig.7 Results of the cooling experiment: (a) selected dip wavelength shift during the cooling cycle (b) dip wavelength shift before the sample is solidified.

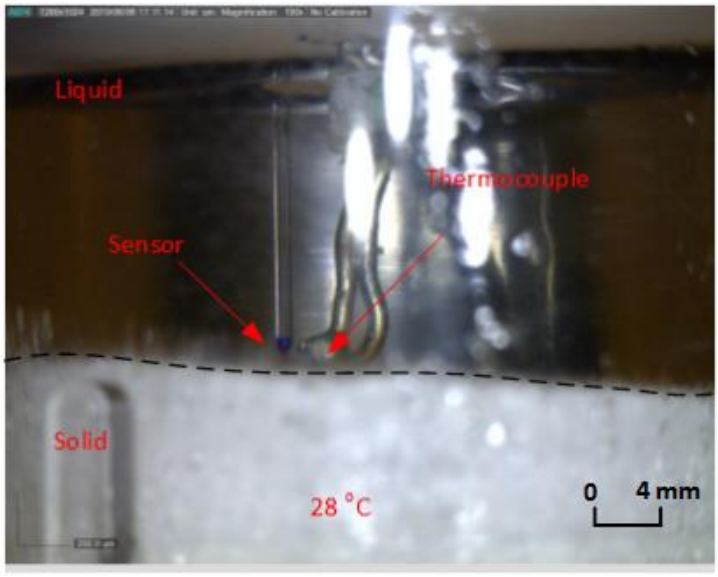

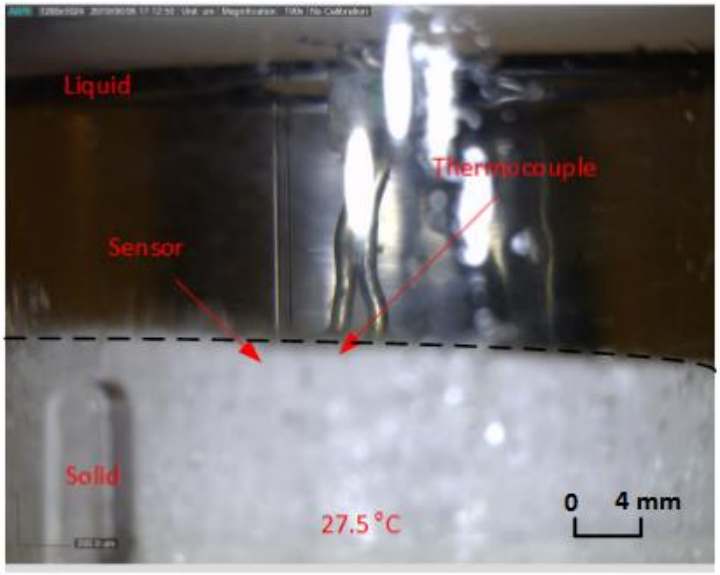

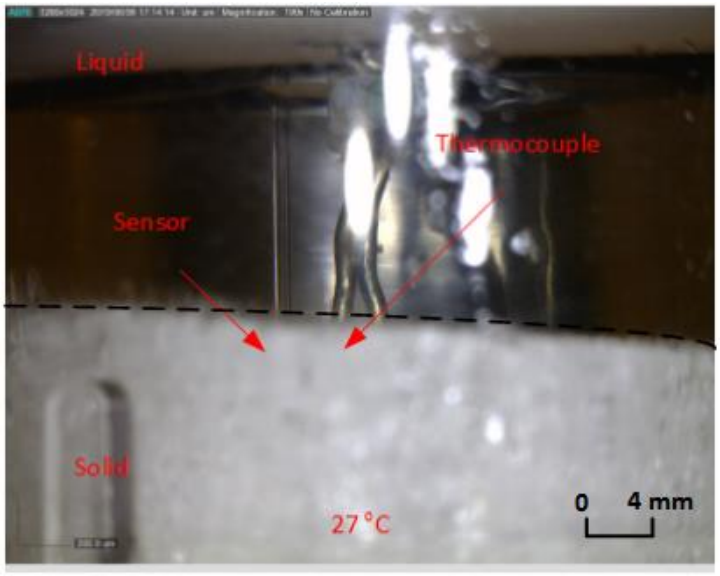

Fig.8 Photographs of the solid-liquid interface position at different temperatures: at 28 °C both the thermocouple and fiber optic probe tips are clearly visible while they are immersed in the solid sample at 27.5ºC.

A side-by-side comparison of the heating and cooling results is shown in Fig. 9. From the figure it can be seen that the wavelength shift in the cooling experiment is larger than the one in the heating experiment. One reason for this is that both the direction and value of the strain and curvature forces acting upon the sensor are different and non-repeatable between heating and cooling cycles.

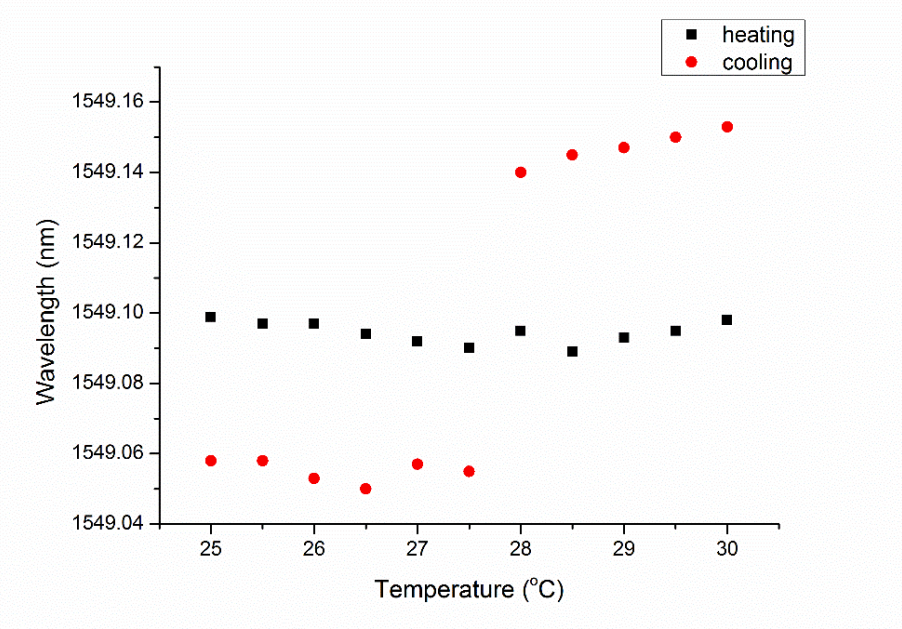

Fig.9 Comparison of the heating and cooling experimental results.

It should be noted that since the proposed method of phase change detection relies on the comparison between the measured slope of the wavelength shift of the selected dip with temperature with the known value of temperature slope in liquid, its accuracy depends on several factors including error of the thermocouple and its position with respect to the material sample. In addition, the measurement sampling interval is an important factor as the accuracy

of detection increases with the increase of the number of consecutive data points used for the linear fitting and comparison of the slopes.

Conclusion

In conclusion, a novel method for in-situ detection of the solid-liquid and liquid-solid phase changes in n-octadecane, based on a Fabry-Perot SHS optical fiber probe has been proposed and demonstrated. From the experimental results it can be seen that the phase change point in the heating experiment is approximately at 28.5 °C on heating and 28 °C on cooling. The accuracy of the phase changes detection was confirmed by visual means. The proposed method allows for a simple, low cost, accurate and reliable in-situ detection of the liquid-solid and solid-liquid phase changes in n-octadecane. The method can be applied to other PCMs. This point-sensing technique can be expanded by increasing the number of sensor probes and can be applied to studies and optimization of heat distribution within PCM materials employed in energy storage systems. And also, it has potential application in modelling of phase changes and can facilitate a better understanding of phase change mechanism.

References

1. Cabeza, L. F. (2014). Advances in Thermal Energy Storage Systems: Methods and Applications. Woodhead Publishing. Hardcover ISBN: 9781782420880.
2. Nagano K., Ogawa, O., Mochida, T., Hayashi, K., Ogoshi, H. (2004). Thermal characteristics of magnesium nitrate hexahydrate and magnesium chloride hexahydrate mixture as a phase change material for effective utilization of urban waste heat. Applied Thermal Engineering, Volume 24, Issues 2–3, 221-232
3. Shmueli, H., Ziskind, G., Letan, R., (2010). Melting in a vertical cylindrical tube: Numerical investigation and comparison with experiments. Int. J. Heat Mass Transfer 53, 4082-4091.
4. Murphy, A. G., Browne, D. J., Mirihanage, W. U., & Mathiesen, R. H. (2013). Combined in situ X-ray radiographic observations and post-solidification metallographic characterisation of eutectic transformations in Al–Cu alloy systems. *Acta Materialia*, *61*(12), 4559-457.
5. Vélez, C., Khayet, M., Ortiz de Zárate, J.M. (2015). Temperature-dependent thermal properties of solid/liquid phase change even-numbered n-alkanes: n-Hexadecane, n-octadecane and n-eicosane. Applied Energy 143, 383–394.
6. Shi, M., Li, S., & Chen, H. (2018). A high-sensitivity temperature sensor based on Sagnac interferometer employing photonic crystal fiber fully filled with ethanol. *Applied Physics B*, *124*(6), 94.
7. Chen, M. Q., Zhao, Y., Xia, F., Peng, Y., & Tong, R. J. (2018). High sensitivity temperature sensor based on fiber air-microbubble Fabry-Perot interferometer with PDMS-filled hollow-core fiber. *Sensors and Actuators A: Physical*, *275*, 60-66.
8. Zhao, X., Zhang, Y., Zhang, W., Li, Z., Kong, L., Yu, L., ... & Yan, T. (2020). Ultra-high sensitivity and temperature-compensated Fabry–Perot strain sensor based on tapered FBG. Optics & Laser Technology, 124, 105997.
9. Sun, Y., Liu, D., Lu, P., Sun, Q., Yang, W., Wang, S., ... & Ni, W. (2017). High sensitivity optical fiber strain sensor using twisted multimode fiber based on SMS structure. Optics Communications, 405, 416-420.

10. Song, D., Chai, Q., Liu, Y., Jiang, Y., Zhang, J., Sun, W., ... & Peng, G. D. (2014). A simultaneous strain and temperature sensing module based on FBG-in-SMS. *Measurement Science and Technology*, *25*(5), 055205.
11. Quan C, Later K, Yang L, Peng S, Zhang A, Hao Q, Zhang J, Sun W, Yuan L and Peng G D 2012 January FBG application in monitoring the liquid-solid and gas-liquid phase transitions of water. In Third Asia Pacific Optical Sensors Conference 8351 835123.
12. Priyadarshini, M., Machavaram, V. R., Sivaramakrishna, A., & Arulmozhivarman, P. (2017). Detecting phase transitions in a $CaCl_2$–H_2O system at low temperatures using a fiber-optic Fresnel reflection sensor. *Applied optics*, *56*(11), 3229-3239.
13. Han, W., Rebow, M., Liu, D., Farrell, G., Semenova, Y., & Wu, Q. (2018). Optical fiber Fresnel reflection sensor for direct detection of the solid–liquid phase change in n-octadecane. *Measurement Science and Technology*, *29*(12), 125107.
14. Han, W., Rebow, M., Lian, X., Liu, D., Farrell, G., Wu, Q., & Semenova, Y. (2019). SNS optical fiber sensor for direct detection of phase transitions in C18H38 n-alkane material. *Experimental Thermal and Fluid Science*, 109854.
15. Choi, M. K. (2016). Using Paraffin PCM to Make Optical Communication Type of Payloads Thermally Self-Sufficient for Operation in Orion Crew Module. In 14th International Energy Conversion Engineering Conference (p. 4601).
16. Mondal, S. (2008). Phase change materials for smart textiles–An overview. *Applied thermal engineering*, *28*(11-12), 1536-1550.
17. Kim, M. S., Kim, M. K., Jo, S. E., Joo, C., & Kim, Y. J. (2016). Refraction-Assisted Solar Thermoelectric Generator based on Phase-Change Lens. *Scientific reports*, *6*, 27913.
18. Vélez, C., Khayet, M., & De Zárate, J. O. (2015). Temperature-dependent thermal properties of solid/liquid phase change even-numbered n-alkanes: n-Hexadecane, n-octadecane and n-eicosane. Applied Energy, 143, 383-394.
19. Wu, C., Liu, Z., Zhang, A. P., Guan, B. O., & Tam, H. Y. (2014). In-line open-cavity Fabry–Pérot interferometer formed by C-shaped fiber fortemperature-insensitive refractive index sensing. *Optics express*, *22*(18), 21757-21766.
20. Chen, Z., Xiong, S., Gao, S., Zhang, H., Wan, L., Huang, X. & Li, Z. (2018). High-Temperature Sensor Based on Fabry-Perot Interferometer in Microfiber Tip. *Sensors*, *18*(1), 202.
21. Chen, M. Q., Zhao, Y., Xia, F., Peng, Y., & Tong, R. J. (2018). High sensitivity temperature sensor based on fiber air-microbubble Fabry-Perot interferometer with PDMS-filled hollow-core fiber. *Sensors and Actuators A: Physical*, *275*, 60-66.
22. Shi, Q., Lv, F., Wang, Z., Jin, L., Hu, J. J., Liu, Z., & Dong, X. (2008). Environmentally stable Fabry–Pérot-type strain sensor based on hollow-core photonic bandgap fiber. *IEEE Photonics Technology Letters*, *20*(4), 237-239.
23. Monteiro, C. S., Ferreira, M. S., Silva, S. O., Kobelke, J., Schuster, K., Bierlich, J., & Frazão, O. (2016). Fiber Fabry-Perot interferometer for curvature sensing. *Photonic Sensors*, *6*(4), 339-344.